

Comparison of Observed Ground-Motion Attenuation for the 16 April 2016 M_w 7.8 Ecuador Megathrust Earthquake and Its Two Largest Aftershocks with Existing Ground-Motion Prediction Equations

by **Céline Beauval, J. Marinière, A. Laurendeau, J.-C. Singaicho, C. Viracucha, M. Vallée, E. Maufroy, D. Mercerat, H. Yepes, M. Ruiz, and A. Alvarado**

ABSTRACT

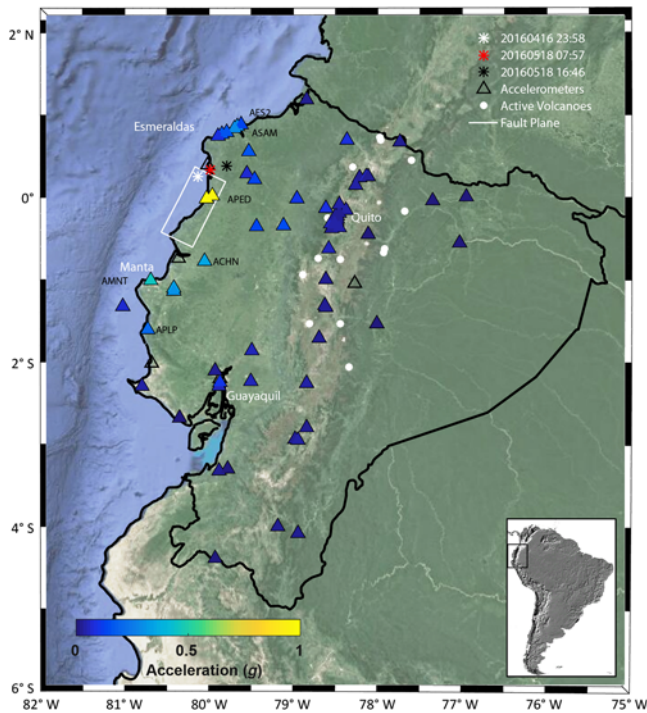
A megathrust subduction earthquake (M_w 7.8) struck the coast of Ecuador on 16 April 2016 at 23:58 UTC. This earthquake is one of the best-recorded megathrust events to date. Besides the mainshock, two large aftershocks have been recorded on 18 May 2016 at 7:57 (M_w 6.7) and 16:46 (M_w 6.9). These data make a significant contribution for understanding the attenuation of ground motions in Ecuador. Peak ground accelerations and spectral accelerations are compared with four ground-motion prediction equations (GMPEs) developed for interface earthquakes, the global Abrahamson *et al.* (2016) model, the Japanese equations by Zhao, Zhang, *et al.* (2006) and Ghofrani and Atkinson (2014), and one Chilean equation (Montalva *et al.*, 2017). The four tested GMPEs are providing rather close predictions for the mainshock at distances up to 200 km. However, our results show that high-frequency attenuation is greater for back-arc sites, thus Zhao, Zhang, *et al.* (2006) and Montalva *et al.* (2017), who are not taking into account this difference, are not considered further. Residual analyses show that Ghofrani and Atkinson (2014) and Abrahamson *et al.* (2016) are well predicting the attenuation of ground motions for the mainshock. Comparisons of aftershock observations with the predictions from Abrahamson *et al.* (2016) indicate that the GMPE provide reasonable fit to the attenuation rates observed. The event terms of the M_w 6.7 and 6.9 events are positive but within the expected scatter from worldwide similar earthquakes. The intraevent standard deviations are higher than the intraevent variability of the model, which is partly related to the poorly constrained V_{S30} proxies. The Pedernales earthquake produced a large sequence of aftershocks, with at least nine events with magnitude higher or

equal to 6.0. Important cities are located at short distances (20–30 km), and magnitudes down to 6.0 must be included in seismic-hazard studies. The next step will be to constitute a strong-motion interface database and test the GMPEs with more quantitative methods.

Electronic Supplement: Figures of V_{S30} values based on topography versus rupture distance and difference between reference V_{S30} and V_{S30} based on topography versus distance, residuals, event terms, and intraevent standard deviations.

INTRODUCTION

The megathrust Pedernales earthquake (M_w 7.8) struck the coast of Ecuador on 16 April 2016 at 23:58 UTC. Sixty-nine accelerometric stations recorded the earthquake at fault distances ranging from 26 to 427 km (Fig. 1). One month after the mainshock, two large aftershocks have been recorded on 18 May 2016 at 7:57 and 16:46 (Table 1; M_w 6.7 and 6.9, respectively). The accelerometric network in Ecuador started in 2009 with nine stations installed in the framework of the French–Ecuadorian research project Andes du Nord (ADN). In 2010, the Ecuadorian research agency Secretaría Nacional de Educación Superior, Ciencia y Tecnología (SENESCYT) granted the Geophysical Institute in Quito with an ambitious project for instrumenting the whole country with high-level instruments, accelerometric, broadband, and Global Positioning System (GPS) stations. The accelerometric network, now called Red Nacional de Acelerógrafos (National Accelerometric Network, RENAC), is



▲ **Figure 1.** Location map with fault rupture and stations. The white rectangle shows the surface projection of the Pedernales mainshock M_w 7.8 (inferred from [Nocquet et al., 2016](#)). Epicenters of the mainshock and its two largest aftershocks are indicated (stars). Triangles show locations of strong-motion stations, which recorded the mainshock and/or the aftershocks. Stations with acceleration indicated (scale bar) recorded the mainshock. Background map produced with Google Maps. The color version of this figure is available only in the electronic edition.

still in a developing phase, with ~30% of the stations telemetered and the characterization of the sites undergoing.

Ecuador is exposed to a high seismic risk, both from earthquakes on the subduction interface, such as the 2016 event, and from earthquakes on shallow crustal faults in the Andean Cordillera. Since 2007, a French–Ecuadorian cooperation aims at

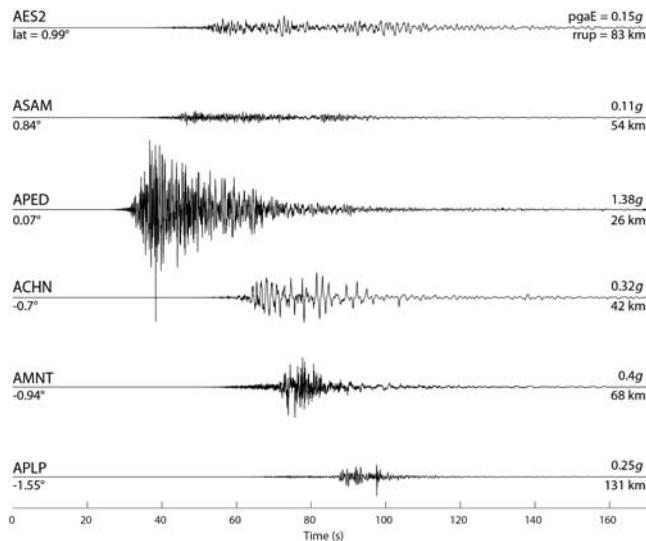
leading research on all aspects related to probabilistic seismic-hazard assessment (PSHA) to improve PSHA in Ecuador (e.g., [Beauval et al., 2010, 2013, 2014](#); [Alvarado et al., 2014](#); [Yepes et al., 2016](#)). PSHA aims at providing ground motions with probabilities of being exceeded in future time windows. The results can be used to establish seismic zoning for national building codes. Because the strong-motion database was still in its development phase, no study has been published yet on the testing of ground-motion prediction equations (GMPEs) against accelerometric data. In the PSHA calculations, GMPEs have been selected based on tectonic similarities criteria (e.g., [Beauval et al., 2014](#)). The M_w 7.8 earthquake and its largest aftershocks produced a unique dataset. These data make a significant contribution for understanding the attenuation of ground motions in Ecuador. In the present study, peak ground accelerations (PGAs) and spectral accelerations are compared with four GMPEs developed for interface earthquakes: the recent global [Abrahamson et al. \(2016\)](#) model as well as two Japanese equations, [Zhao, Zhang, et al. \(2006\)](#) and [Ghofrani and Atkinson \(2014\)](#), and a new Chilean model ([Montalva et al., 2017](#)).

STRONG-MOTION DATA

Strong-motion data are obtained from the RENAC, which includes seven accelerometers from the Oleoducto de Crudos Pesados network as well as nine ADN accelerometers. Figure 1 shows the distribution of the 69 stations triggered by the Pedernales event relative to the earthquake fault-plane surface projection. There are 16 stations at rupture distances ranging from 26 to 100 km, distributed in the coastal plain. Thirty-three stations are located in the north–south Andean Cordillera hosting many volcanoes, and 14 stations are installed in the Quito basin ([Laurendeau et al., 2017](#)). Approximately half of the stations are located in the fore-arc region, west of the volcanic front, and the other half lie in the back-arc region. The records at six example stations are displayed in Figure 2. The M_w 6.9 and 6.7 aftershocks were recorded, respectively, by 61 and 64 stations; 5 of these stations did not record the mainshock (Fig. 1).

Date (yyyy/mm/dd)	Time (UTC) (hh:mm)	Hypocenter Latitude (°)	Hypocenter Longitude (°)	Hypocenter Depth (km)	Fault Strike (°)	Dip Angle (°)	Fault Length (km)	Fault Width (km)	M_w Global CMT*
2016/04/16	23:58	0.35 [†]	80.17 [†]	17 [†]	26.5 [†]	23 [†]	110 [†]	60 [†]	7.8
2016/05/18	07:57	0.43387 [‡]	−80.00961 [‡]	17 [‡]	29 [‡]	26 [‡]	28 [§]	30 [§]	6.7
2016/05/18	16:46	0.47301 [‡]	−79.81545 [‡]	21 [‡]	47 [‡]	25 [‡]	36 [§]	34 [§]	6.9

*Obtained from the Global Centroid Moment Tensor Project (Global CMT; see [Data and Resources](#)).
[†]Deduced from [Nocquet et al. \(2016\)](#).
[‡]Determined by Geophysical Institute in Quito (dip and strike obtained with [Nakano et al., 2008](#) method).
[§]Determined with the scaling law for interface events in [Strasser et al. \(2010\)](#).



▲ **Figure 2.** Pedernales earthquake on 16 April 2016 M_w 7.8. Accelerograms recorded at six stations around the fault plane (see Fig. 1, east component). Latitudes of stations, maximum amplitude, and rupture distance to the fault plane are indicated.

All stations are installed on the ground surface and record continuously. Different digital accelerometer devices are used (Güralp, RefTek, and Kinometrics; see Table 2). For this study, a simple processing was applied. Acceleration time histories were visually inspected and windows extracted. A first-order baseline operator and a simple baseline correction are applied on each window for each component. Signal-to-noise Fourier spectral ratios have been carefully calculated with the signal processing tools of Perron *et al.* (2016). Given the magnitude of the three events, these ratios are, in most cases, high for the frequencies of interest (PGA and 0.5–5 Hz). At the stations located at distances between 300 and 500 km, the signal-to-noise ratios are still higher or equal to 3 in this frequency range. Response spectra were then calculated with critical damping at 5%. For each record, the geometric-mean horizontal component is calculated for PGA and spectral periods up to 3 s.

The site conditions at a recording station have a strong influence on ground motions. The most common proxy for the simplified classification of a site in terms of its seismic

response is V_{S30} , the time-average shear-wave velocity in the upper 30 m. In Ecuador, few RENAC stations have been characterized with geophysical methods, and significant efforts still need to be made to evaluate the geotechnical information of the sites. In Quito (14 sites), V_{S30} are inferred from geophysical investigations of the subway project (TRX Consulting C.A., 2011a, b) and from a microzoning study (Evaluacion de Riesgos Naturales [ERN], 2012). For each station, V_{S30} is inferred from the shear-wave velocity profile closest to the site. In Guayaquil (three sites), V_{S30} values come from the work of Vera-Grunauer (2014). A new project was started after the mainshock by the Geophysical Institute to investigate the site effects in the coastal cities, which to this date yields V_{S30} values for three sites based on multichannel analysis of surface waves techniques.

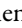
For the other sites, following Zhao, Irikura, *et al.* (2006), horizontal-to-vertical (H/V) response spectral ratios are computed to determine the natural period of the site (T_g) and to classify the sites into four broad site classes (SC I, II, III, IV, from rock to soft soil). The number of recordings available at each station varies from 3 to 203 (15 on average, see Laurendeau *et al.*, 2016). The entire signal windows are used. At 33 sites, the natural period can be estimated, and V_{S30} is deduced as $V_{S30} = 4H/T_g$, with $H = 30$ m. At 16 sites with a natural period estimated higher or equal to 0.6 s (soft soil, SC IV, Zhao, Zhang, *et al.*, 2006), V_{S30} is fixed to 200 m/s. At six sites showing a flat H/V ratio with amplitudes lower than 2, the site is classified in the rock and stiff soil class with a V_{S30} of 800 m/s. There are 14 sites for which there was no clear peak but broadband frequency amplification. The method cannot be applied, and an average V_{S30} of 400 m/s is arbitrarily attributed. More work is required to understand the limits of the method and how to adapt it to sites in Ecuador. This set of estimated V_{S30} is considered as the reference V_{S30} set (Fig. 3).

To take into account the huge uncertainty on the V_{S30} values, a second set of V_{S30} is used. It is based on the weighting of the four closest points given in the database on the Global U.S. Geological Survey V_{S30} Slope Topography website (see Data and Resources). These V_{S30} are based on a relationship between the topographic slope and V_{S30} (Wald and Allen, 2007). The V_{S30} values based on topography are compared with the reference V_{S30} values in Figure S1 (available in the electronic supplement to this article). At

Table 2
Description of Red Nacional de Acelerógrafos (National Accelerometric Network, RENAC) Accelerometer Devices

	Sensor	Digitizer	Full-Scale Range (g)	Dynamic Range	Frequency Response (Hz)	Sample Frequency (Hz)
1	Güralp CMG-5TD		±4	127 dB at 3–30 Hz	DC–100	100
2	RefTek 130-SMA		±4	112 dB at 1 Hz	DC–500	100
3	Kinometrics EpiSensor FBA ES-T	Kephren	±2	155 dB	DC–200	125 or 250

DC, direct current.

distances shorter than 100 km, in the fore-arc region, the difference does not exceed 200 m/s. At larger distances, up to 600 m/s, difference can be observed for stations in the Cordillera. In the present work, the comparisons between observations and predictions are systematically led for both V_{S30} sets, showing that this uncertainty does not impact the results. All results displayed in the article rely on the reference V_{S30} set, whereas results based on the alternative V_{S30} set based on topography are in the  electronic supplement.

GMPEs SELECTED

GMPEs describe the median and the variability of ground-motion amplitudes, depending on magnitude, site-source distance, site conditions, and other parameters. Four equations are considered here, two Japanese models, one Chilean, and one global model: Zhao, Zhang, *et al.* (2006), Ghofrani and Atkinson (2014), Montalva *et al.* (2017), and Abrahamson *et al.* (2016). The Zhao, Zhang, *et al.* (2006) model does not include the recent interface events but proved to be quite stable and to fit reasonably the data available in South America (e.g., Arango *et al.*, 2012; Beauval, Cotton, *et al.*, 2012). The Abrahamson *et al.* (2016) model is our favorite candidate for PSHA applications, because it includes the largest amount of global data, and an earlier version of the model proved to be stable and to fit well datasets from various subduction environments (Beauval, Cotton, *et al.*, 2012). All four models use the geometric mean of the two horizontal components, moment magnitude, and rupture distance (closest distance to the fault plane). All are providing the total sigma, as well as the intraevent (variability from the median-predicted value for a particular recording station in a given earthquake) and interevent variabilities (variability between earthquakes of the same magnitude).

The Abrahamson *et al.* (2016) model is based on the combined datasets used in several of the past subduction GMPEs (e.g., Youngs *et al.*, 1997; Atkinson and Boore, 2003), as well as additional ground-motion data obtained in Japan, Taiwan, south and central America, and Mexico. This new global GMPE is intended to replace the older global GMPEs. The metadata were carefully checked and improved, and recent events around the world were included. The final dataset includes 43 interface earthquakes ($6.0 \leq M_w \leq 8.4$) at distances up to 300 km. About 57% interface records are from Japan and 29% from Taiwan. The model is predicting a stronger attenuation for sites located in the back-arc region with respect to sites located in the fore-arc region. The model is including site nonlinearity.

Ghofrani and Atkinson (2014) developed a GMPE for interface earthquakes of M_w 7.0–9.0, based on data from Japan. The > 600 strong ground motion records from the 2011 M_w 9.0 Tohoku earthquake are used to derive an event-specific GMPE, which is then extended to represent the shaking from four other $M_w > 7.0$ interface events in Japan, which occurred in 2003, 2004, and 2005. Three GMPEs are finally available to represent the epistemic uncertainty, an upper and lower model, as well as a median model. The median central model is used

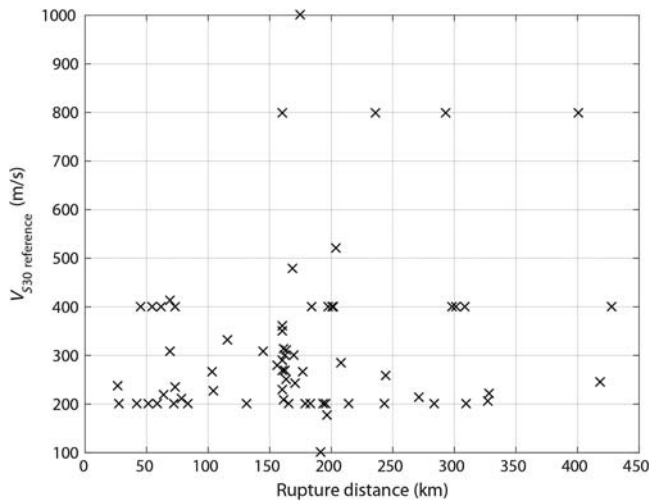
here. The equation accounts for the difference in the attenuation between fore-arc and back-arc region using separate anelastic attenuation factors. The soil response is treated as linear. Ghofrani and Atkinson (2014), like Abrahamson *et al.* (2016), explicitly use V_{S30} .

Zhao, Zhang, *et al.* (2006) developed an attenuation model for Japan based on events with M_w 5.0–8.3, at distances up to 300 km. Four site classes are used in the present study, SC I, II, III and IV, approximately corresponding to the four classes, rock, hard soil, medium soil, and soft soil (site classification scheme used in Japanese engineering design; Zhao, Zhang, *et al.*, 2006). The authors associated with these site classes approximate National Earthquake Hazards Reduction Program (NEHRP) site classes and V_{S30} intervals (table 2 in Zhao, Zhang, *et al.*, 2006). The near-source data (< 30 km) are mostly constrained by the records from crustal events; however, this should not affect the predictions for subduction events for distances > 30 km.

Montalva *et al.* (2017) developed a GMPE relying on Chilean subduction earthquakes that occurred between 1985 and 2015, including the three recent megathrust earthquakes (2010 M_w 8.8 Maule, 2014 M_w 8.1 Iquique, and 2015 M_w 8.3 Illapel). The median model is based on the same functional form as the Abrahamson *et al.* (2016) model. The attenuation is predicted only for fore-arc sites, because all recording stations are located in the fore-arc region. Montalva *et al.* (2017) indicate that the number of strong-motion stations with measured V_{S30} is limited and that V_{S30} proxies have been inferred both from the topographic slope (Wald and Allen, 2007) and the site's predominant period (Zhao, Irikura, *et al.*, 2006). Montalva *et al.* (2017), like Abrahamson *et al.* (2016) and Zhao, Zhang, *et al.* (2006), do not include data beyond 300 km.

Abrahamson *et al.* (2016) and Ghofrani and Atkinson (2014) predict different attenuation depending on the location of the station with respect to the volcanic front. The fore-arc region is between the subduction trench axis and the axis of volcanic front. The back-arc region is behind the volcanic front. The high-attenuation low-velocity region in the crust and upper mantle related to the volcanic activity filters the high-frequency content of ground motion, as shown by Ghofrani and Atkinson (2011) on in-slab events and by Ghofrani and Atkinson (2014) on interface events.

Most of the interface models published up to now have been coded in the strong-motion toolkit used here for predicting accelerations (Weatherill, 2014). This toolkit relies on the GMPE libraries of the OpenQuake PSHA software (Pagani *et al.*, 2014). The Lin and Lee (2008) GMPE established on Taiwanese data was not selected because the equation is using the hypocentral distance, and given the short distances involved in Ecuador this might not be adequate. The Kanno *et al.* (2006) GMPE is not included because it would be a third Japanese model, and it uses an unconventional definition for the horizontal component of motion. The Mexican equation by Arroyo *et al.* (2010) is not considered either because it predicts ground motions at rock sites only (NEHRP B class).



▲ **Figure 3.** V_{S30} reference set versus rupture distance (see the [Strong-Motion Data](#) section). Alternative V_{S30} values based on topography are in © [Figure S1](#), available in the electronic supplement to this article.

FAULT-PLANE SOLUTION AND DISTANCE CALCULATION

The site-source distances are calculated using the closest distance to the fault rupture plane (rupture distance). The fault must be approximated by a rectangular plane. There is no unique solution for the finite-fault plane (e.g., [Goda and Atkinson, 2014](#)). Different fault models can be derived using various datasets and methods in source inversion analysis. The inversion might include GPS data, Interferometric Synthetic Aperture Radar, teleseismic body wave, surface-wave data, and near-source strong-motion data. [Goda and Atkinson \(2014\)](#) explored the uncertainty related to the choice of the rupture plane for three Japanese megathrust earthquakes and showed that the impact on the comparison between observations and models can be significant. For now, for the 2016 Pedernales event, we are aware of only one elaborated model by [Nocquet et al. \(2016\)](#). The maximum slip is about 6.2 m. From this slip model, we extracted the fault plane, which includes approximately the 100-cm slip contour. The resulting plane is a rectangular of 100 km in length and 50 km in width, dipping to the east with a strike of 26.50° and a dip of 23° , extending from 13 to 33 km ([Table 1](#); [Fig. 1](#)). The hypocenter solution is up-dip on the northern border of the fault plane.

The Pedernales earthquake is one of the best-recorded megathrust events to date, in terms of distribution of stations around the fault plane and number of recording stations. Records are available above the fault plane (two stations, [Fig. 1](#)), at short distances from the fault plane to the north and northeast (10 stations between 45 and 100 km), east (2 stations at 73 and 103 km), and south and southeast (4 stations between 40 and 75 km).

The rupture distance measure, taking into account the extension of the fault plane, only captures macroscopic features of the source. The more detailed components of recorded strong motions in the near-source region are not taken into account (e.g., short periods affected by local asperities). Besides, the 2016 Pedernales event is presenting evidences of directivity effects, with higher ground motions in the direction of the slip, south of the rupture plane, than in the north. These observations cannot be modeled by current published interface GMPEs.

Because no fault-plane solution has been inverted yet for the aftershocks, the length and width of the faults are based on a [Strasser et al. \(2010\)](#) relations ([Table 1](#)). The fault plane is arbitrarily centered on the hypocenter.

COMPARING OBSERVATIONS AND PREDICTIONS

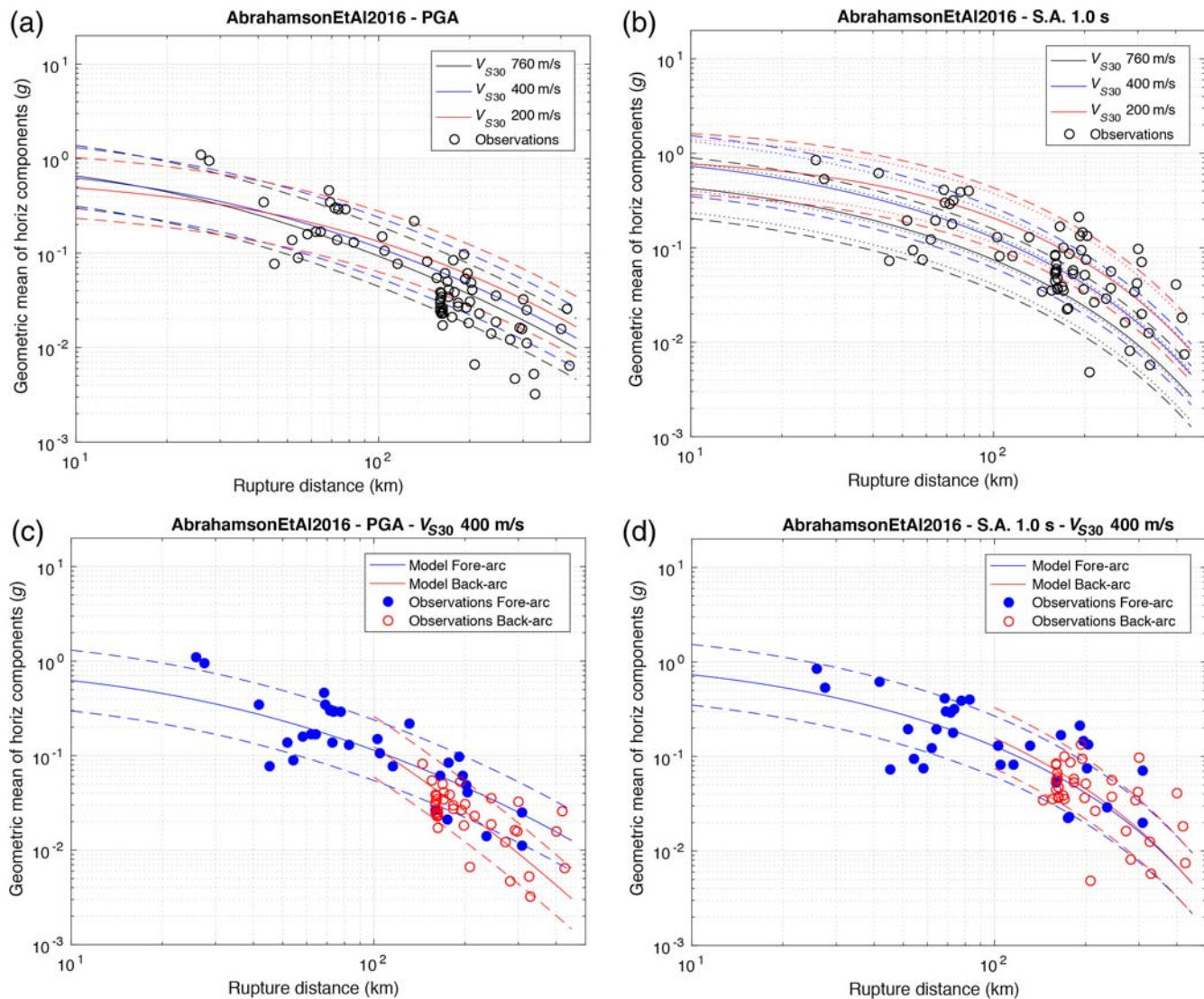
Mainshock M_w 7.8

At first, predictions and observations are compared based on simple attenuation plots. As a second step, residual analyses are performed in which the predictions include the V_{S30} for each site.

Predictions from [Abrahamson et al. \(2016\)](#) are superimposed onto the observations, for the PGA ([Fig. 4a](#)). To begin with, predictions are provided with the fore-arc/unknown option ([Abrahamson et al., 2016](#)). Three V_{S30} are considered (200, 400, and 760 m/s), producing slightly different amplitudes. The attenuation rate predicted is consistent with the observations for distances lower or equal to 130 km. For distances between 130 and 400 km, the observed attenuation rate appears steeper than predicted. Stations within 130 km from the rupture plane are all in the fore-arc region. At distances larger than 130 km, half of the stations are within or behind the volcanic arc ([Fig. 1](#)). Taking into account the back-arc option in the equation yields a steeper attenuation with distance, in accordance with the observations at back-arc stations ([Fig. 4c](#)). In Quito, located at around 150 km from the earthquake in the Cordillera ([Fig. 1](#)), recorded PGA varies between 0.017g and 0.081g.

The rupture propagated to the south, producing directivity effects on ground motions. At rupture distances 40–80 km, stations located to the south of the rupture experienced larger amplitudes than stations located to the north or to the east ([Figs. 1 and 5](#)). A specific study will need to be performed to investigate the source contribution on the Pedernales ground motions. The recorded data might need to be corrected for path and site effects to explain the difference of amplitudes in terms of source directivity (see, e.g., [Cultrera et al., 2008](#)).

As expected, long-period ground motions decay less rapidly with distance than do short-period motions. [Figure 4b](#) displays predictions superimposed on observations at $T = 1.0$ s. Amplitudes predicted are more V_{S30} dependent than for short periods. Overall, the attenuation rate predicted is consistent with observations. Considering predictions for V_{S30} from 200 to 760 m/s and considering the predicted variability (total sigma), most of the observations are within the predicted range.

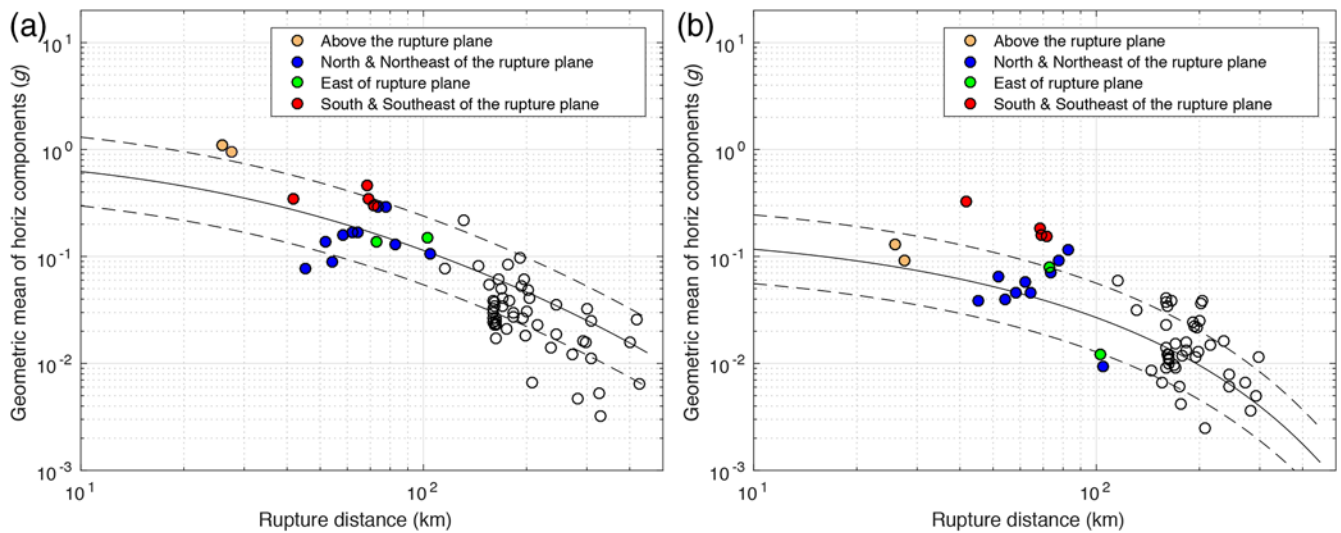


▲ **Figure 4.** Observed spectral amplitudes of the mainshock M_w 7.8, overlaid by the [Abrahamson et al. \(2016\)](#) predicted amplitudes (median $\pm\sigma$). Total sigma is indicated with dashed lines. (a) Peak ground acceleration (PGA) for three different V_{S30} values, fore-arc/unknown coefficients used for all stations; (b) spectral acceleration $T = 1.0$ s for three different V_{S30} values, fore-arc/unknown coefficients used for all stations; (c) PGA predictions for fore-arc sites and for back-arc sites for a V_{S30} of 400 m/s; (d) spectral acceleration $T = 1.0$ s predictions for fore-arc sites and for back-arc sites for a V_{S30} of 400 m/s. The color version of this figure is available only in the electronic edition.

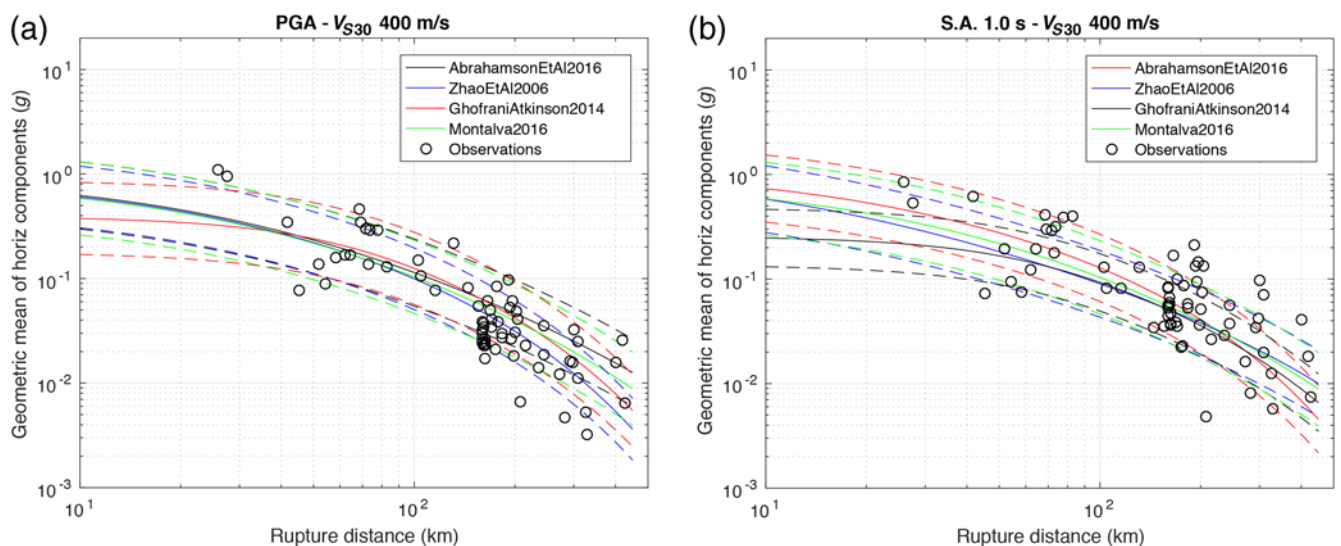
The model predicts similar decay with distance for fore-arc and back-arc regions, and the observations indeed do not present significant differences (Fig. 4d).

Predictions by [Zhao, Zhang, et al. \(2006\)](#), [Ghofrani and Atkinson \(2014\)](#), and [Montalva et al. \(2017\)](#) are now superimposed onto the observed data, considering an average V_{S30} value (400 m/s, Fig. 6). For distances in the 30–150 km range, PGA median predictions from the four GMPEs are quite similar and consistent with the observed attenuation rate, with around 0.3g predicted at 40 km and 0.1g–0.11g at 100 km. The total sigma predicted are also close. For distances larger than 150 km, the two Japanese models predict stronger distance decay. The [Zhao, Zhang, et al. \(2006\)](#)

model does not differentiate attenuation between fore-arc and back-arc stations, but its generating dataset includes many Japanese back-arc stations. Applying the fore-arc/back-arc station classification, the [Ghofrani and Atkinson \(2014\)](#) model predicts a stronger attenuation for back-arc stations at distances larger than 100 km, with predictions very close to the [Abrahamson et al. \(2016\)](#) model (Fig. 7a, PGA). At $T = 1.0$ s, the [Abrahamson et al. \(2016\)](#) model predicts larger accelerations at distances < 200 km than the Japanese and Chilean models (Fig. 6b). The generating datasets of [Abrahamson et al. \(2016\)](#), [Zhao, Zhang, et al. \(2006\)](#), and [Montalva et al. \(2017\)](#) do not include records beyond 300 km, and the models are therefore extrapolated at these distances.



▲ **Figure 5.** Evidence of directivity effects at (a) PGA and (b) 3 s. The stations located at rupture distances lower or equal to 100 km are highlighted, and their location with respect to the fault plane is indicated. Abrahamson *et al.* (2016) predicted amplitudes with $V_{S30} = 400$ m/s (see legend of Fig. 4a). The color version of this figure is available only in the electronic edition.

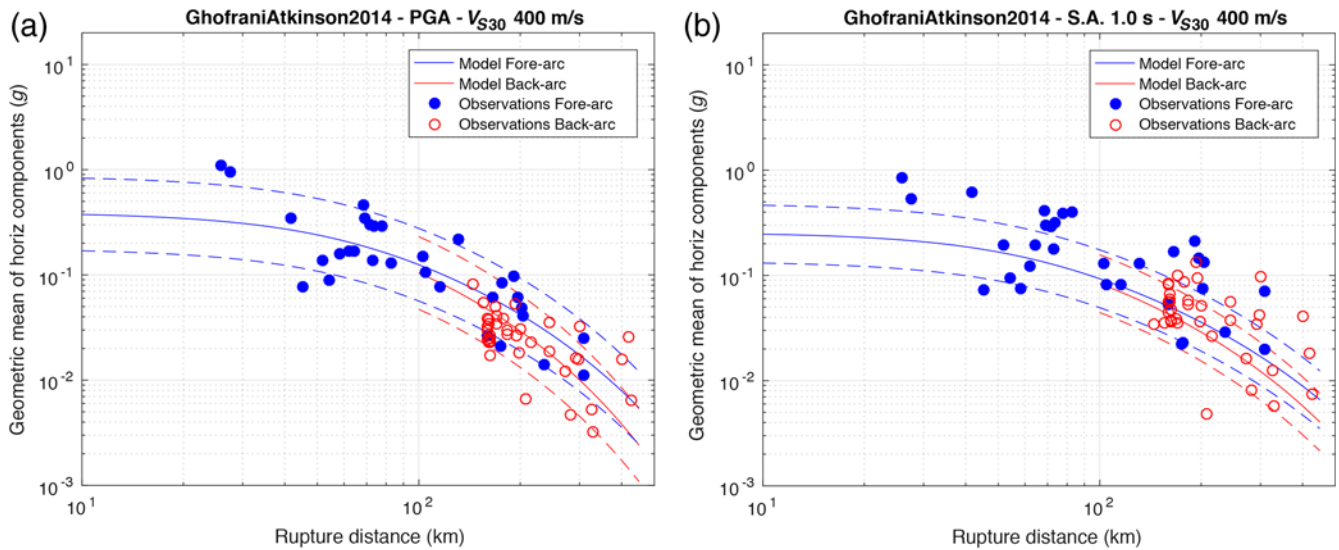


▲ **Figure 6.** Observed spectral amplitudes of the mainshock M_w 7.8 at (a) PGA and (b) spectral acceleration $T = 1.0$ s, overlaid by four ground-motion prediction equation (GMPE) curves: Abrahamson *et al.* (2016), Ghofrani and Atkinson (2014), Zhao, Zhang, *et al.* (2006), and Montalva *et al.* (2017). Total sigma is indicated with dashed lines. Predictions for an average V_{S30} of 400 m/s. The color version of this figure is available only in the electronic edition.

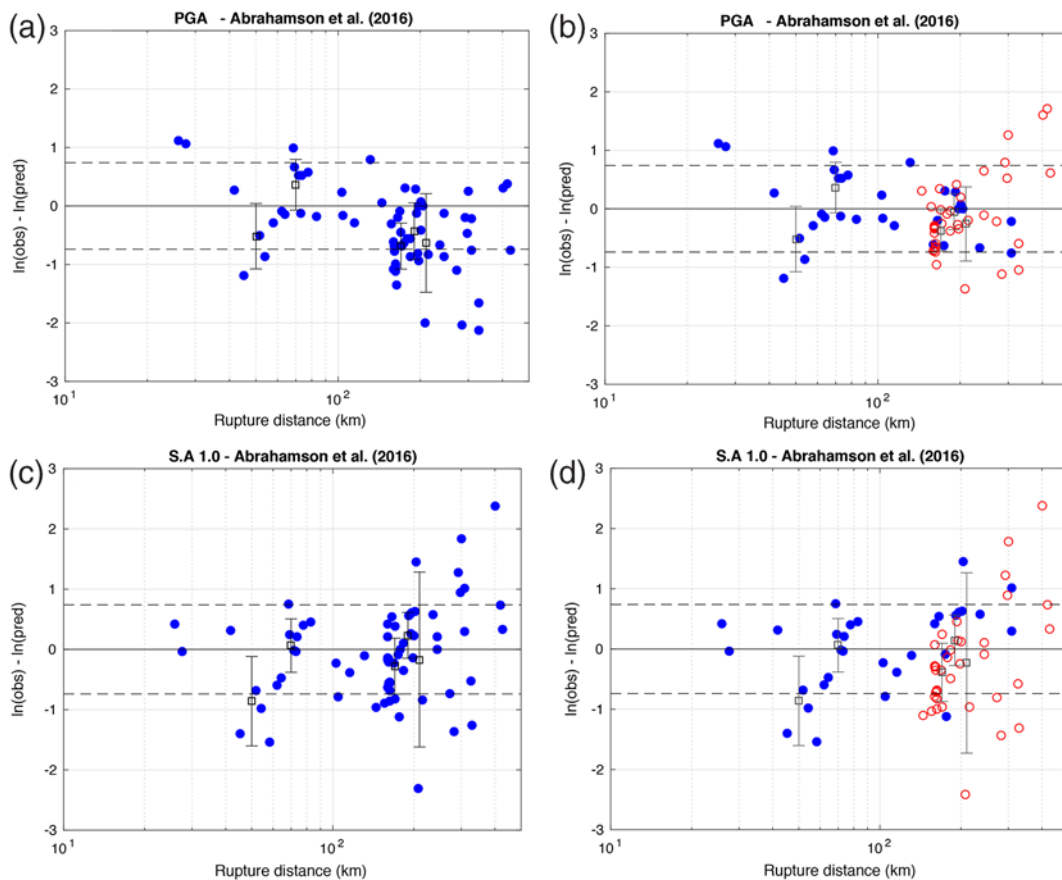
To more accurately evaluate the performance of the GMPEs relative to the data, total residuals are calculated considering V_{S30} for each station (V_{S30} reference set, see the [Strong-Motion Data](#) section). Residuals are calculated first ignoring the fore-arc/back-arc distinction, and then including this attenuation difference. At the PGA, a trend in the distance dependence of residuals is observed with back-arc sites showing a negative slope (Fig. 8a). Applying back-arc coefficient to the sites in the back-arc region, the slope becomes flatter, with mean residuals closer to zero (Fig. 8b). The same observation can be made for the residuals relative to the equa-

tion of Ghofrani and Atkinson (2014) (Ⓔ Fig. S2). At 1 s, as expected, no difference can be seen in the distance-decay rates for the fore-arc and the back-arc stations (Fig. 8c,d). The Ghofrani and Atkinson (2014) model is slightly underestimating the observations, as shown by the mean residuals higher or equal to zero.

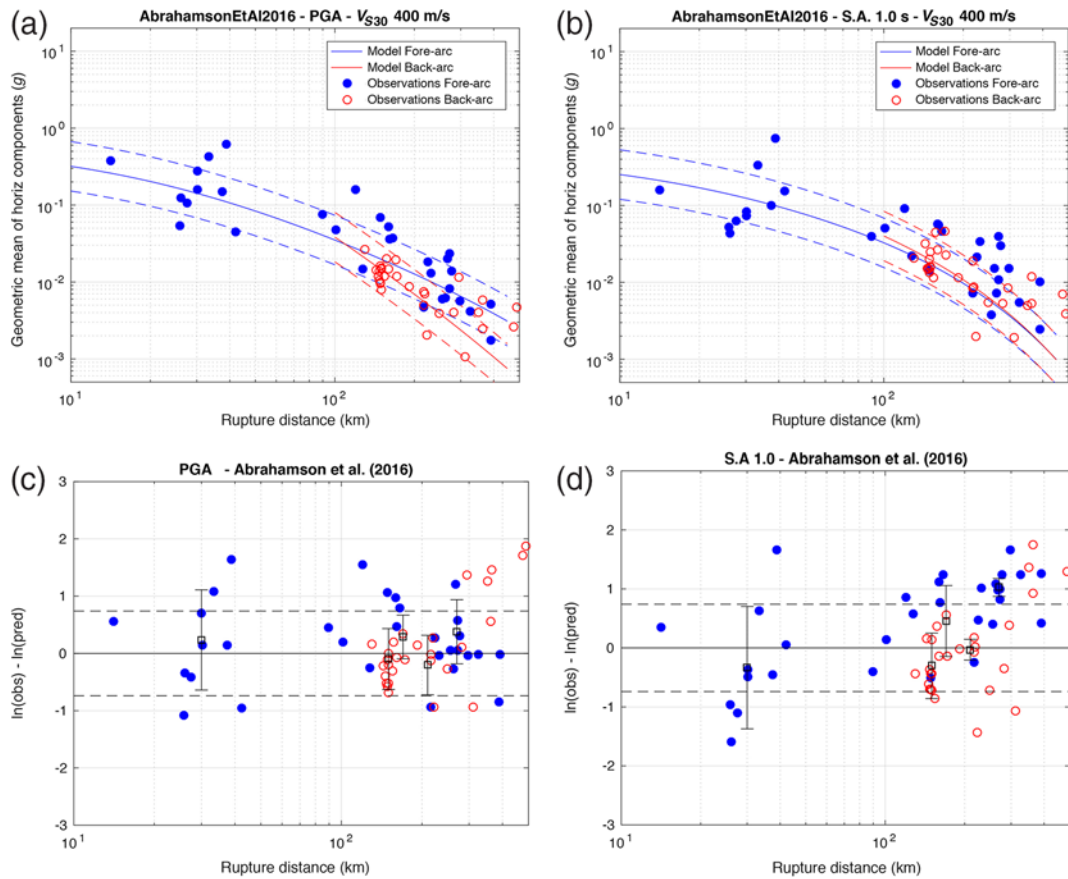
At present, the uncertainty on V_{S30} estimate is huge for the RENAC stations (see the [Strong-Motion Data](#) section). The second set of V_{S30} values based on topographic slope is considered as an attempt to evaluate the impact of V_{S30} uncertainty on the results. The residuals obtained with the Abrahamson *et al.*



▲ **Figure 7.** Observed spectral amplitudes of the mainshock M_w 7.8 overlaid by the Ghofrani and Atkinson (2014) predicted amplitudes (median $\pm\sigma$), for (a) PGA and (b) spectral acceleration $T = 1.0$ s, for an average V_{S30} of 400 m/s. The color version of this figure is available only in the electronic edition.



▲ **Figure 8.** Total residuals, mainshock, the Abrahamson *et al.* (2016) model. The residuals are binned into intervals of 20 km width, and the corresponding means (squares) and standard deviations (bars) are displayed when calculated on at least four values. Dashed lines indicate \pm total sigma (0.74). Event term is the mean of the residuals. V_{S30} reference set considered (see the Strong-Motion Data section). Abrahamson *et al.* (2016) generating dataset does not include records beyond 300 km, and the model is therefore extrapolated at these distances. The color version of this figure is available only in the electronic edition.



▲ **Figure 9.** Aftershock on 16 May 2016 M_w 6.9 at 16:46. (a) and (b) Attenuation of PGA and spectral accelerations at $T = 1.0$ s with distance and comparison to [Abrahamson *et al.* \(2016\)](#) GMPE for an average V_{S30} of 400 m/s. (c) and (d) Total residuals of data relative to [Abrahamson *et al.* \(2016\)](#) model; residuals binned in 20-km-width intervals and displayed if calculated over more than four observations; dashed lines indicates \pm total sigma. [Abrahamson *et al.* \(2016\)](#) generating dataset does not include records beyond 300 km, and the model is therefore extrapolated at these distances. The color version of this figure is available only in the electronic edition.

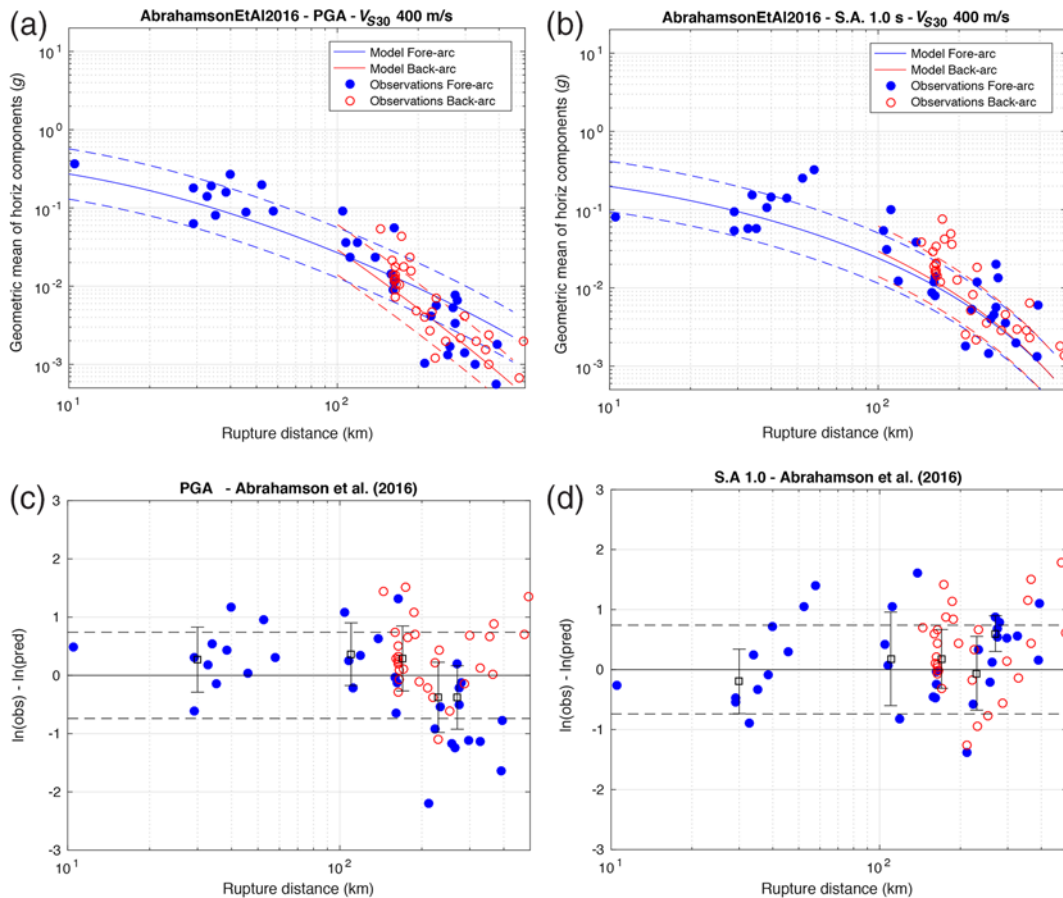
(2016) model are presented in [Figure S3](#). Residuals are quite stable with respect to the previous ones. At the PGA, for distances lower than 100 km, residuals are identical to the ones calculated with the reference V_{S30} set. This is expected; at these distances the difference in the V_{S30} values is not exceeding 200 m/s ([Figure S1](#)). At larger distances, only slight difference in the mean residuals can be noticed. At spectral period $T = 1.0$ s, the mean of residuals is slightly shifted to positive values with respect to [Figure 8](#), but still no major change is observed. Throughout the study, all residuals have been derived on both sets of V_{S30} values, showing that the results are stable.

Aftershocks M_w 6.9 and 6.7

Because the mainshock data show clearly an attenuation effect due to wave passage through the volcanic front, the models applied in Ecuador should take this difference into account. The equation of [Ghofrani and Atkinson \(2014\)](#) is made for events with magnitude higher than 7.0. Thus, only the [Abrahamson *et al.* \(2016\)](#) model is considered further for the aftershocks.

[Figure 9](#) shows geometric mean PGA and $T = 1.0$ s spectral acceleration as a function of rupture distance for the M_w 6.9 event. The median and sigma predicted by the [Abrahamson *et al.* \(2016\)](#) model are superimposed onto the data, for an average V_{S30} value of 400 m/s. The residuals are also calculated. Observations are more scattered than for the mainshock; however, comparable observations can be made. The attenuation rate predicted is roughly consistent with the observations, with a stronger attenuation at back-arc sites for PGA. Mean of residuals are in general within one standard deviation. At $T = 1.0$ s, mean residuals at distances larger than 150 km are larger or equal to sigma, indicating that the model is predicting a stronger attenuation than observed.

Results for the M_w 6.7 aftershocks are displayed in [Figure 10](#). At short period (PGA), the difference in attenuation between fore-arc and back-arc stations is less clear ([Figure 10a](#)). The attenuation rate for back-arc sites appears to better fit the observations for distances larger than 100 km for all stations (fore-arc and back-arc). Residuals indeed show a negative slope ([Figure 10c](#)). The residuals at $T = 1.0$ s show a flatter slope, with



▲ **Figure 10.** Aftershock on 18 May 2016 M_w 6.7 at 7:57. (a) and (b) Attenuation of PGA and spectral accelerations at $T = 1.0$ s with distance and comparison to Abrahamson *et al.* (2016) GMPE for an average V_{S30} of 400 m/s. (c) and (d) Total residuals of data relative to Abrahamson *et al.* (2016) model; residuals binned in 20-km-width intervals and displayed if calculated over more than four observations; dashed lines indicates \pm total sigma. Abrahamson *et al.* (2016) generating dataset does not include records beyond 300 km, and the model is therefore extrapolated at these distances. The color version of this figure is available only in the electronic edition.

positive mean residuals at distances larger than 100 km, indicating that the model is predicting, on average, lower ground motions than observed (Fig. 10d). Part of the data is indeed above the predictions (Fig. 10b).

Event Terms and Intraevent Standard Deviations

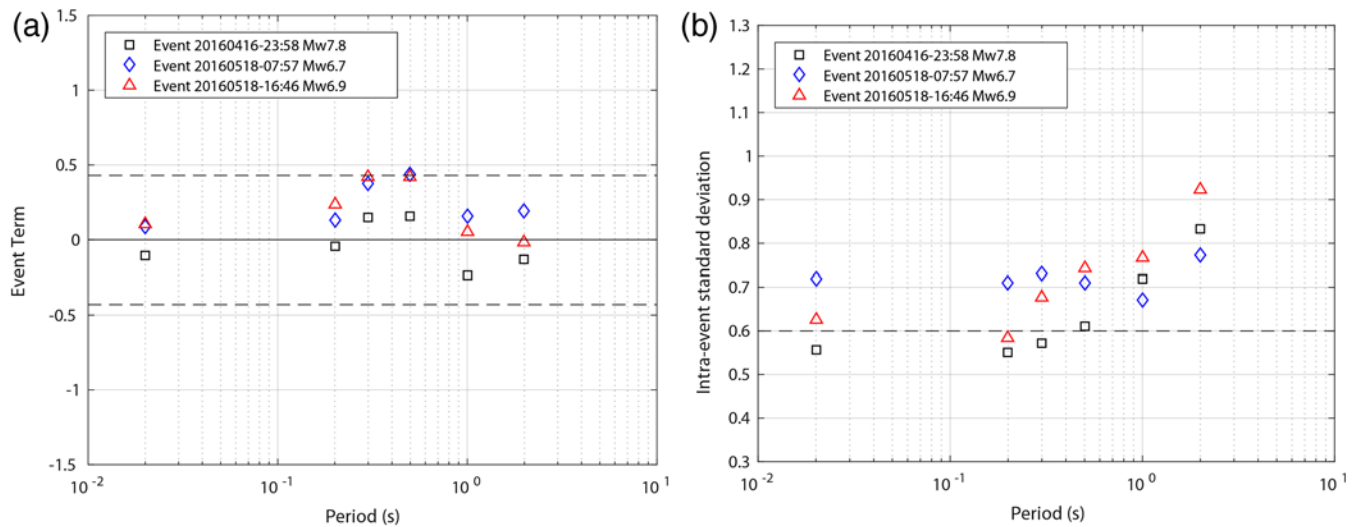
For the three events, the event term and intraevent standard deviations are calculated for a suite of six periods between PGA and 2 s (Fig. 11). Residuals at distances larger than 300 km, the validity limit of the Abrahamson *et al.* (2016) model, are not included. The event term is the mean of the residuals in a single event over all stations. The intraevent residual is the misfit between an individual observation at a station from the earthquake-specific median prediction, which is defined as the median prediction of the model plus the event term for the earthquake (Al Atik *et al.*, 2010). The general trend of the event terms with spectral period is consistent for the three earthquakes (Fig. 11a). Event terms are mostly within the expected scatter for interface subduction earthquakes worldwide ($\tau = 0.43$). Event terms are both neg-

ative and positive for the mainshock but always positive for the aftershocks (larger than expected ground motions). Intraevent standard deviations for the mainshock are close to the expected scatter ($\phi = 0.6$) for spectral periods lower than 1 s (Fig. 11b). At 1 and 2 s, the intraevent variability is higher than expected. This might be partly due to the poorly constrained V_{S30} parameter and to the directivity effects on the ground motions.

Residuals, event terms, and intraevent standard deviations based on the second set of V_{S30} values, relying on topography, are displayed in ⊕ Figures S4 and S5. Results are quite stable with respect to the calculations based on the reference V_{S30} . Intraevent standard deviations are again higher or equal to the intraevent variability predicted by the model.

CONCLUSIONS

The Pedernales interface earthquake of 16 April 2016 produced a unique dataset which enables us to analyze the attenuation of ground motion with distance in Ecuador and to evaluate the per-



▲ **Figure 11.** (a) Event terms of the Pedernales mainshock and its two largest aftershocks, compared to the [Abrahamson et al. \(2016\)](#) interevent standard deviation τ (0.43); (b) intraevent standard deviation for Pedernales mainshock and its two largest aftershocks compared to the [Abrahamson et al. \(2016\)](#) intraevent standard deviation ϕ (0.6). Recordings at distances larger than 300 km are not included. Results for PGA are indicated at the frequency 50 Hz. The color version of this figure is available only in the electronic edition.

formance of interface models currently in use to predict strong ground motions in seismic-hazard studies. The national accelerometric network RENAC is young, and most stations still require site characterization, limiting the precision in the comparison of observations with existing ground-motion models.

The four considered GMPEs, [Zhao, Zhang, et al. \(2006\)](#), [Ghofrani and Atkinson \(2014\)](#), [Montalva et al. \(2017\)](#), and [Abrahamson et al. \(2016\)](#), are providing rather close predictions for an M_w 7.8 earthquake at distances up to 200 km. However, our results show that high-frequency attenuation is greater in the back-arc region, thus [Zhao, Zhang, et al. \(2006\)](#) and [Montalva et al. \(2017\)](#), which are not taking into account this difference, are not considered further. Overall, residual analyses show that the [Ghofrani and Atkinson \(2014\)](#) and [Abrahamson et al. \(2016\)](#) models are rather well predicting the attenuation of ground motions for the mainshock, both for short and long periods. A specific study investigating the signature of directivity effects in the recorded ground motions remains to be done.

Comparisons of aftershock observations with the [Abrahamson et al. \(2016\)](#) predictions indicate that the GMPE provides a reasonable fit to the attenuation rates observed. The event terms of the M_w 6.7 and 6.9 events are positive but within the expected scatter from worldwide similar earthquakes. The intraevent standard deviations are higher than the intraevent variability of the model, which is partly related to the poorly constrained V_{S30} proxies.

The Pedernales earthquake produced a large sequence of aftershocks, with at least nine events with magnitude equal to or higher than 6.0 recorded to date. Because the coast is close to the trench and the slab dip is shallow, important cities are

located at short distances (20–30 km), and magnitudes down to 6.0 must be included in seismic-hazard studies. The next step will be to constitute a strong-motion interface database and test the GMPEs with more quantitative methods (e.g., [Scherbaum et al., 2009](#); [Beauval, Tasan, et al., 2012](#)). Onsite measurements of velocity using geophysical techniques have begun and are planned for all RENAC sites. In a year or two, hopefully, the site conditions of the stations will be much better known.

DATA AND RESOURCES

The accelerometric dataset was recorded by the National Accelerometric Network of Ecuador (RENAC) maintained by the Geophysical Institute, Escuela Politécnica Nacional, Quito, and by the Oleoducto de Crudos Pesados (OCP) network. The Global Centroid Moment Tensor Project database was searched using www.globalcmt.org/CMTsearch.html (last accessed August 2016). The OpenQuake Ground Motion Toolkit is available online at <https://github.com/GEMScienceTools/gmpe-smtk> (last accessed August 2016). The programs developed by D. Boore to calculate fault-to-station distances are available online at http://www.daveboore.com/software_online.html (last accessed August 2016). The global V_{S30} Map Server was searched using <http://earthquake.usgs.gov/hazards/apps/vs30/> (last accessed August 2016). ✉

ACKNOWLEDGMENTS

This work was supported by the Instituto Geofísico, Escuela Politécnica Nacional, Quito, by the Institut de Recherche pour

le Développement (IRD), Centre national de la recherche scientifique–Institut national des sciences de l’Univers (CNRS-INSU), and by the Agence Nationale de la Recherche through the project REMAKE (Grant Number ANR-15-CE04-004). On the Ecuadorian side, additional support was available from the Secretaría Nacional de Educación Superior, Ciencia y Tecnología (SENESCYT; LAE-5 y Proyecto PIN_08-EPNGEO-00001). This work has been carried out in the frame of the Joint International Laboratory “Seismes & Volcans dans les Andes du Nord” (IRD LMI SVAN). Previous funding from the Agence Nationale de la Recherche of France is acknowledged (Grant Number ANR-07-BLAN-0143-01). We also acknowledge the Oleoducto de Crudos Pesados (OCP) for the use of their accelerometric data. We thank Dave Boore for sharing his programs to calculate fault-to-station distances and Gonzalo Montava for sharing his MATLAB script to predict ground motions with the new Chilean ground-motion prediction equation (GMPE). We are also grateful to Graeme Weatherhill and the Global Earthquake Model Modeling Facility for constant support on OpenQuake. At last, we would like to acknowledge Pierre-Yves Bard for fruitful interactions and discussions, as well as two anonymous reviewers for their constructive comments.

REFERENCES

- Abrahamson, N., N. Gregor, and K. Addo (2016). BC hydro ground motion prediction equations for subduction earthquakes, *Earthq. Spectra* **32**, no. 1, 23–44.
- Al Atik, L., N. Abrahamson, J. J. Bommer, F. Scherbaum, F. Cotton, and N. Kuehn (2010). The variability of ground-motion prediction models and its components, *Seismol. Res. Lett.* **81**, no. 5, 794–801, doi: [10.1785/gssrl.81.5.794](https://doi.org/10.1785/gssrl.81.5.794).
- Alvarado, A., L. Audin, J. M. Nocquet, S. Lagreulet, M. Segovia, Y. Font, G. Lamarque, H. Yepes, P. Mothes, F. Rolandone, *et al.* (2014). Active tectonics in Quito, Ecuador, assessed by geomorphological studies, GPS data, and crustal seismicity, *Tectonics* **33**, no. 2, 67–83, doi: [10.1002/2012TC003224](https://doi.org/10.1002/2012TC003224).
- Arango, M., F. Strasser, J. Bommer, J. Cepeda, R. Boroschek, D. Hernandez, and H. Tavera (2012). An evaluation of the applicability of current ground-motion models to the south and central American subduction zones, *Bull. Seismol. Soc. Am.* **102**, 143–168.
- Arroyo, D., D. Garcia, M. Ordaz, M. A. Mora, and S. K. Singh (2010). Strong ground-motion relations for Mexican interplate earthquakes, *J. Seismol.* **14**, 769–785.
- Atkinson, G. M., and D. M. Boore (2003). Empirical ground-motion relations for subduction-zone earthquakes and their application to Cascadia and other regions, *Bull. Seismol. Soc. Am.* **93**, no. 4, 1703–1729.
- Beauval, C., F. Cotton, N. Abrahamson, N. Theodulidis, E. Delavaud, L. Rodriguez, F. Scherbaum, and A. Haendel (2012). Regional differences in subduction ground motions, *World Conf. on Earthquake Engineering*, Lisbon, Portugal, 24–28 September, 10 pp.
- Beauval, C., H. Tasan, A. Laurendeau, E. Delavaud, F. Cotton, P. Guéguen, and N. Kuehn (2012). On the testing of ground-motion prediction equations against small magnitude data, *Bull. Seismol. Soc. Am.* **102**, no. 5, 1994–2007.
- Beauval, C., H. Yepes, L. Audin, A. Alvarado, J.-M. Nocquet, D. Monelli, and L. Danciu (2014). Probabilistic seismic hazard assessment in Quito, estimates and uncertainties, *Seismol. Res. Lett.* **85**, no. 6, doi: [10.1785/0220140036](https://doi.org/10.1785/0220140036).
- Beauval, C., H. Yepes, W. Bakun, J. Egred, A. Alvarado, and J.-C. Singaicho (2010). Locations and magnitudes of historical earthquakes in the Sierra of Ecuador (1587–1996), *Geophys. J. Int.* **181**, no. 3, 1613–1633, doi: [10.1111/j.1365-246X.2010.04569.x](https://doi.org/10.1111/j.1365-246X.2010.04569.x).
- Beauval, C., H. Yepes, P. Palacios, M. Segovia, A. Alvarado, Y. Font, J. Aguilar, L. Troncoso, and S. Vaca (2013). An earthquake catalog for seismic hazard assessment in Ecuador, *Bull. Seismol. Soc. Am.* **103**, 773–786, doi: [10.1785/0120120270](https://doi.org/10.1785/0120120270).
- Cultrera, G., F. Pacor, G. Franceschina, A. Emolo, and M. Cocco (2008). Directivity effects for moderate-magnitude earthquakes (M_w 5.6–6.0) during the 1997 Umbria–Marche sequence, central Italy, *Tectonophysics* **476**, nos. 1/2, doi: [10.1016/j.tecto.2008.09.022](https://doi.org/10.1016/j.tecto.2008.09.022).
- Evaluacion de Riesgos Naturales (ERN) (2012). Microzonificacion sismica del distrito metropolitano de Quito: estudio de la amenaza sismica a nivel local, *Informe Final*, 198 pp. (in Spanish).
- Goda, K., and G. Atkinson (2014). Variation of source-to-site distance for megathrust subduction earthquakes: Effects on ground motion prediction equations, *Earthq. Spectra* **30**, no. 2, 845–866.
- Ghofrani, H., and G. Atkinson (2011). Forearc versus backarc attenuation of earthquake ground motion, *Bull. Seismol. Soc. Am.* **101**, 3032–3045.
- Ghofrani, H., and G. Atkinson (2014). Ground-motion prediction equations for interface earthquakes of M 7 to M 9 based on empirical data from Japan, *Bull. Earthq. Eng.* **12**, 549–571.
- Kanno, T., A. Narita, N. Morikawa, H. Fujiwara, and Y. Fukushima (2006). A new attenuation relation for strong ground motion in Japan based on recorded data, *Bull. Seismol. Soc. Am.* **96**, no. 3, 879–897.
- Laurendeau, A., L. F. Bonilla, D. Mercerat, F. Courboux, A. Alvarado, J. C. Singaicho, P. Guéguen, and E. Bertrand (2017). Seismic response of the basin of Quito from continuous accelerometric records of RENAC-Quito, *16th World Conf. on Earthquake Engineering*, Santiago, Chile, January 2017, 11 pp., Extended Abstract.
- Laurendeau, A., M. Perrault, D. Mercerat, L.-F. Bonilla, F. Courboux, C. Beauval, J.-G. Barros, F. Vasconez, J. Marinière, J.-C. Singaicho, *et al.* (2016). Preliminary observations of site effects during the M_w 7.8 Pedernales (Ecuador) earthquake on April 16th 2016, *5th IASPEI/LAEE International Symposium: Effects of Surface Geology on Seismic Motion*, Taipei, Taiwan, 15–17 August, 12 pp.
- Lin, P.-S., and C.-T. Lee (2008). Ground-motion attenuation relationships for subduction-zone earthquakes in northeastern Taiwan, *Bull. Seismol. Soc. Am.* **98**, no. 1, 220–240.
- Montalva, G., N. Bastias, and A. Rodriguez-Marek (2017). Ground motion prediction equation for the Chilean subduction zone, *Bull. Seismol. Soc. Am.* **107**, no. 2, doi: [10.1785/0120160221](https://doi.org/10.1785/0120160221).
- Nakano, M., H. Kumagai, and H. Inoue (2008). Waveform inversion in the frequency domain for the simultaneous determination of earthquake source mechanism and moment function, *Geophys. J. Int.* **173**, 1000–1011, doi: [10.1111/j.1365-246X.2008.03783.x](https://doi.org/10.1111/j.1365-246X.2008.03783.x).
- Nocquet, J.-M., P. Jarrin, M. Vallée, P. A. Mothes, R. Grandin, F. Rolandone, B. Delouis, H. Yepes, Y. Font, D. Fuentes, *et al.* (2016). Supercycle at the Ecuadorian subduction zone revealed after the 2016 Pedernales earthquake, *Nature Geosci.* doi: [10.1038/ngeo2864](https://doi.org/10.1038/ngeo2864).
- Pagani, M., D. Monelli, G. Weatherill, L. Danciu, H. Crowley, V. Silva, P. Henshaw, L. Butler, M. Nastasi, L. Panzeri, *et al.* (2014). OpenQuake-engine: An open hazard (and risk) software for the global earthquake model, *Seismol. Res. Lett.* **85**, 692–702.
- Perron, V., C. Gélis, F. Hollender, P.-Y. Bard, B. Froment, E. M. Cushing, and G. Cultrera (2016). Broadband site effect assessment: comparison between approaches based on earthquakes and microtremors on two sites, *5th IASPEI/LAEE International Symposium:*

- Effects of Surface Geology on Seismic Motion*, Taipei, Taiwan, 15–17 August.
- Scherbaum, F., E. Delavaud, and C. Riggelsen (2009). Model selection in seismic hazard analysis: An information-theoretic perspective, *Bull. Seismol. Soc. Am.* **99**, no. 6, 3234–3247.
- Strasser, F. O., M. C. Arango, and J. J. Bommer (2010). Scaling of the source dimensions of interface and intraslab subduction-zone earthquakes with moment magnitude, *Seismol. Res. Lett.* **81**, 941–950.
- TRX Consulting C.A. (2011a). *Estudio de Caracterización de Ruta con Métodos Geofísicos no Invasivos*, TRX Consulting C.A. (in Spanish).
- TRX Consulting C.A. (2011b). *Aplicación Métodos Geofísicos en Caracterización de Sitio*, TRX Consulting C.A. (in Spanish).
- Vera-Grunauer, X. (2014). Seismic response of a soft, high plasticity, diatomaceous naturally cemented clay deposit, Ph.D. dissertation, University of California, Berkeley, 909 pp.
- Wald, D. J., and T. I. Allen (2007). Topographic slope as a proxy for seismic site conditions and amplification, *Bull. Seismol. Soc. Am.* **97**, no. 5, 1379–1395.
- Weatherill, G. A. (2014). OpenQuake ground motion toolkit—User guide, *Global Earthquake Model (GEM). Technical Report*, 88 pp.
- Yepes, H., L. Audin, A. Alvarado, C. Beauval, J. Aguilar, Y. Font, and F. Cotton (2016). A new view of Ecuador’s geodynamic context and its implications for seismogenic sources definition and seismic hazard assessment, *Tectonics* **35**, doi: [10.1002/2015TC003941](https://doi.org/10.1002/2015TC003941).
- Youngs, R. R., S. J. Chiou, W. J. Silva, and J. R. Humphrey (1997). Strong ground motion attenuation relationships for subduction zone earthquakes, *Seismol. Res. Lett.* **68**, no. 1, 58–73.
- Zhao, J. X., K. Irikura, J. Zhang, Y. Fukushima, P. G. Somerville, A. Asano, Y. Ohno, T. Oouchi, T. Takahashi, and H. Ogawa (2006). An empirical site-classification method for strong-motion stations in Japan using H/V response spectral ratios, *Bull. Seismol. Soc. Am.* **96**, no. 3, 914–925.
- Zhao, J. X., J. Zhang, A. Asano, Y. Ohno, T. Oouchi, T. Takahashi, H. Ogawa, K. Irikura, H. K. Thio, P. G. Somerville, *et al.* (2006). Attenuation relations of strong ground motion in Japan using site classification based on predominant period, *Bull. Seismol. Soc. Am.* **96**, no. 3, 898–913.

Céline Beauval
 J. Marinière
 E. Maufroy
 ISTERre, Université Grenoble Alpes, IRD, CNRS, OSUG
 CS 40700
 38058 Grenoble, CEDEX 9
 France
celine.beauval@univ-grenoble-alpes.fr

A. Laurendeau
 J.-C. Singaicho
 C. Viracucha
 H. Yepes
 M. Ruiz
 A. Alvarado
 Escuela Politecnica Nacional
 Instituto Geofísico
 Ladrón de Guevara E11-253, Apartado 2759
 Quito 170143, Ecuador

M. Vallée
 Institut de Physique du Globe de Paris
 1 Rue Jussieu, 75005 Paris
 France

D. Mercerat
 CEREMA
 56, Boulevard Stalingrad
 06359 Nice, CEDEX 4
 France

Published Online 15 February 2017